A Probabilistic Approach for Contact Stability and Contact Safety Analysis of Robotic Intracardiac Catheter

Ran Hao *
Department of Electrical, Computer,
and Systems Engineering Engineering
Case Western Reserve University
Cleveland, Ohio 44106
Email: rxh349@case.edu

M. Cenk Çavuşoğlu
Department of Electrical, Computer,
and Systems Engineering Engineering
Case Western Reserve University
Cleveland, Ohio 44106
Email: mcc14@case.edu

The disturbances caused by the blood flow and tissue surface motions are major concerns during the motion planning of a intracardiac robotic catheter. Maintaining a stable and safe contact on the desired ablation point is essential for achieving effective lesions during the ablation procedure. In this paper, a probabilistic formulation of the contact stability and the contact safety for intravascular cardiac catheters under the blood flow and surface motion disturbances is presented. Probabilistic contact stability and contact safety metrics, employing a sample based representation of the blood flow velocity distribution and the heart motion trajectory, are introduced. Finally, the contact stability and safety for a MRI-actuated robotic catheter under main pulmonary artery blood flow disturbances and left ventricle surface motion disturbances are analyzed in simulation as example scenarios.

1 Introduction

The focus of this paper is on the analysis of contact stability and contact safety of a robotic intravascular cardiac catheter under blood flow and surface motion disturbances given tip position constraint on the tissue surface. Specifically, a stable contact ensures no slippage between the catheter-tip and the tissue surface under given disturbances, and a safe contact ensures the normal contact force to remain within the desired force limits under given disturbances. In this study, the MRI-actuated robotic catheter [1, 2] designed for performing intra-vascular cardiac interventions is used as the underlying example robotic catheter platform. A probabilistic blood flow model is formulated, where the blood flow drag forces applied on the catheter body is approximated using a quasi-static model, assuming the blood flow to be constant and uniform within a small time interval. The probabilistic contact stability and contact safety metrics, employing the sample based representation of the blood flow velocity distribution or the heart motion trajectory, are then proposed. Finally, the contact stability and contact safety of the robotic catheter are analyzed using the proposed models and metrics, where the left pulmonary inferior vein (LIV) blood flow and left ventricle heart surface motions are used as two example disturbances. To the best of our knowledge, this is the first work that presents a probabilistic framework for modeling and evaluating the contact quality under the influences of blood flow disturbances and heart surface motion disturbances.

The quality of the contact force between the catheter tip and the tissue surface is critical for effective lesion formation [3–5]. Several studies suggest that contact force <10 g will result in atrial fibrillation recurrence [3–5]. However, excessively high contact forces would cause complications including steam pop, acute tissue edema, perforation, and thrombus formation [4]. Thiagalingam et al. [4] propose that a "moderate" catheter contact force of 20 g can increase the possibility of more effective lesions. Williams et al. [6] suggest that high contact force > 25 g may lead to heating and edema of extracardiac structures. In this study, the desired

*This work was supported in part by the National Science Foundation under grants CISE IIS-1524363, CISE IIS-1563805, ENG IIP-1700839, and National Heart, Lung, and Blood Institute of the National Institutes of Health under grant R01 HL153034. This paper was presented in part at the 2020 IEEE International Conference on Intelligent Robots and Systems (IROS 2020), Las Vegas, USA.

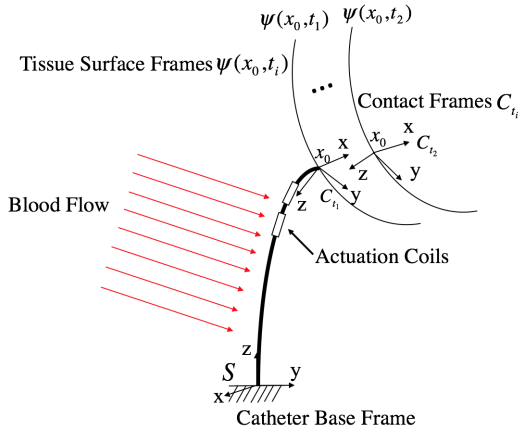

Fig. 1. The MRI-actuated robotic catheter with two sets of tri-axial actuation coils subject to the perturbation forces resulting from blood flow drag forces and the tissue surface constraint. The catheter base frame S is given as shown. The contact frame C_{t_i} is chosen such that its origin is located at the contact point of the catheter and the z-axis is the outward normal of the tissue surface at time t_i. x_0 denotes the contact point position in surface frame, which remains static during heart surface motion. $\Psi(x_0,t_i)$ denotes the parametrization of tissue surface given contact point x_0 at time t_i.

normal contact force is restricted to the range from 10 g to 25 g (0.1 N∼0.25 N), and the ability of the robotic catheter to maintain the normal contact force in this narrow therapeutic range given blood flow or heart motion disturbances is investigated.

This paper presents an extended version of the contact stability and contact safety analysis framework proposed by the authors in [7]. In the original work presented in [7], the probabilistic contact stability and safety models are evaluated only under the influence of blood flow disturbances. This paper extends this framework by including the probabilistic contact stability and contact stability metrics under heart surface motion disturbances. In addition, the contact model is formulated independent of the catheter kinematic model in this paper.

The rest of this paper is organized as follows. The blood flow drag forces, the contact force under surface constraint and under the blood flow drag forces are modeled in Section 2. The probabilistic contact stability and contact safety metrics are introduced in Section 3. The simulation based contact stability and safety analysis are presented in Section 4. Finally, the simulation results are discussed and conclusions are drawn in Section 5.

2 Contact Model of Catheter

2.1 Contact Force and Contact Ratio

In this section, the catheter tip-tissue contact model is formulated. The origin of the contact frame is located at the contact point, and its z-axis is in the outward surface normal direction, as indicated by Fig. 1. The contact between the catheter tip and the tissue surface is assumed as point contact with friction (non-conforming), the contact Jacobian $J_C \in \mathbb{R}^{3\times n}$ relating contact forces to joint torques is given by [8]:

$$J_C = \frac{\partial x_c}{\partial X}, \tag{1}$$

where $x_c \in \mathbb{R}^3$ denotes the position of the catheter tip in contact frame, $X \in \mathscr{C}$ represent the catheter configuration in configuration space $\mathscr{C}$. Let λ_c denote the magnitude of the normal contact force, λ_f denote the tangential forces. The friction cone defines the set of "stable" contact forces which cause no slippage between the tip and the surface, which is given as:

$$FC = \{f_c \in \mathbb{R}^3 \ : \ \sqrt{{\lambda_{f1}}^2 + {\lambda_{f2}}^2} \leq \mu_s \lambda_c\}, \tag{2}$$

where f_c denotes the contact force in the contact frame and $f_c = [\lambda_{f1}, \lambda_{f2}, \lambda_c]$, μ_s denotes the static friction coefficient [8].

Let $u \in \mathbb{R}^m$ represent the actuation of the robotic catheter. The relationship between the catheter configuration and the actuation under the tip contact position constraint is described by minimizing the potential energy of the catheter subjected to the given constraint. For example, in the pseudo-rigid-body model proposed by [9], the potential energy function $f(u,X)$ is given as:

$$\min_X \frac{1}{2} X^T K X - \sum_i F_i^T p_i(X) - \sum_j B_j(X)^T \mu_j(u_j) \tag{3}$$

$$\text{s.t. } g(X, \Psi(x_0)) = 0. \tag{4}$$

In this model, $X \in \mathbb{R}^n$ denotes the pseudo joint configuration, K is the stiffness matrix, F_i denotes a conservative force acting on the catheter at $p_i(X)$, B_j is the MRI's magnetic field vector written in the j-th actuator frame, and μ_j is the magnetic moment of the j-th actuator expressed in its body frame, The constraint function $g : \mathbb{R}^n \times \mathbb{R}^3 \to \mathbb{R}^3$ is defined as $h(X) - \Psi(x_0)$, such that the catheter tip is at the desired tip position on the surface. $\Psi : \mathbb{R}^2 \to \mathbb{R}^3$ maps a point from surface frame to spatial frame (Fig. 1), and $\Psi(x_0)$ denotes the desired tip position in spatial frame. $h(X) \in \mathbb{R}^3$ denotes the forward kinematics of the catheter.

The Lagrangian $\mathscr{L} : \mathbb{R}^m \times \mathbb{R}^n \to \mathbb{R}$ can be used to set up the optimization problem presented in (3). The equation of the Lagrangian $\mathscr{L}$ is given as [9]:

$$\mathscr{L} : \ f(u, X) - g^T \lambda \tag{5}$$

where λ is the Lagrange multiplier.

From (3)-(5) and (1), the equilibrium equation $\nabla \mathscr{L}$ at given catheter-tissue contact configuration can be expressed

as [9]:

$$\nabla \mathscr{L} : \nabla_X f(u,\, X) - J_C^T f_c = 0, \tag{6}$$

and the contact force is then calculated as:

$$f_c = J_C^{T^\dagger} \nabla_X f(u,\, X), \tag{7}$$

where $J_C^{T^\dagger}$ is the left pseudo-inverse of J_C^T with $J_C^{T^\dagger} = (J_C J_C^T)^{-1} J_C$. The contact ratio σ_μ between friction force and normal force is defined as:

$$\sigma_\mu = \frac{\|\lambda_f\|}{\lambda_c}, \tag{8}$$

where $\sigma_\mu \in \mathbb{R}$. The friction coefficient between the catheter tip and the tissue surface is denoted as μ_s. Then for contact forces with $0 \leq \sigma_\mu \leq \mu_s$, the contact force will remain inside the friction cone FC and the catheter can sustain a stable contact with the tissue surface at the target contact position.

2.2 Contact Model with Blood Flow Disturbances

Periodic blood flow passing through the left atrium will exert drag forces on the robotic catheter. Accurately modeling the blood flow inside the heart and the resulting drag forces on the catheter in their full complexity would not be computationally feasible to be used as part of a robotic catheter control scheme. Therefore, in this study, a simplified blood flow drag force model is employed. Specifically, the blood flow drag forces acting on the catheter will be modeled as probabilistic perturbation forces. The set of perturbation forces and their associated probabilities are estimated using a quasi-steady flow model. A distribution of blood flow velocities is generated from a temporal sampling of the blood flow velocity profile observed at the pulmonary veins from where the blood enters into the left atrium. Then the distribution of blood flow drag forces is calculated using these samples of blood flow velocities, approximating the flow to be steady and uniform within the small time interval containing the given velocity sample. Since the flows in the left atrium and great vessels are generally fast and dominated by inertial forces rather than viscous forces [10], the friction drag and the viscous drag can be ignored, and the pressure drag f_b per unit length of the catheter body at a point x can be calculated as [11]:

$$f_b(x,v) = \frac{1}{2}\rho C_D d v^2 w_{v,n}(x). \tag{9}$$

Since the catheter is moved rather slowly by the physician during ablation for proper lesion formation, v is approximately the speed of the fluid. d is the outer diameter of the catheter, C_D is the drag coefficient which is correlated to the dimensional ratio [11], and ρ is the density of the blood. $w_v \in \mathbb{R}^{3x1}$ is the direction vector of the blood flow velocity in spatial frame, with $||w_v|| = 1$, and $w_{v,n}(x)$ denotes the normal component of the direction vector that is orthogonal to the catheter body at x.

Suppose the blood flow exerts on the catheter segment of $[s,l]$, the blood flow drag can be incorporated in the equilibrium equation (6) as an external load $F_b(X,v)$:

$$F_b(X,v) = \int_s^l J(x)^T f_b(x,v) dx. \tag{10}$$

where $J(x)^T$ maps the blood flow drag at x to configuration space. As the computation of $F_b(X,v)$ is model-dependent, we refer the readers to [7] and [12] for detailed information. The contact force under blood flow disturbance is then expressed as:

$$f_c = J_C^{T^\dagger}(\nabla_X f(u,\, X) - F_b(X,v)). \tag{11}$$

3 Probabilistic Contact Stability and Contact Safety Metrics

Given disturbance samples, the stability of the catheter-tissue contact is quantified using the probabilistic contact stability metric:

$$\kappa_\sigma = P(0 \leq \sigma_\mu \leq \mu_s), \tag{12}$$

namely, the probability that the contact force between the catheter tip and the tissue surface remains inside the friction cone FC, under the given disturbances. Similarly, the safety of the catheter's contact with the tissue surface is quantified using the probabilistic contact safety metric:

$$\kappa_f = P(f_{\min} \leq f_{\text{normal}} \leq f_{\max}). \tag{13}$$

In this paper, sample based representations are used to represent the blood flow and contact ratio probability distributions for more easily accommodating non-Gaussian probability distributions and non-linear transformations [13]. First, the samples of the blood flow velocity distribution, $\{v^{[1]},\ v^{[2]},\ ...,\ v^{[N_v]}\}$, are drawn from the blood flow velocity probability density function p_v, i.e., $v^{[j]} \sim p_v$. The corresponding contact ratio samples $\{\sigma_\mu^{[1]},\ \sigma_\mu^{[2]},\ ...,\ \sigma_\mu^{[N_v]}\}$, which represent the probability distribution of the contact ratio, p_{σ_μ}, are then obtained from $v^{[j]}$ using (8) and (11). Specifically, from (11),

$$f_c^{[j]} = J_C^{T^\dagger}(\nabla_X f(u,\, X) - F_b(X, v^{[j]})). \tag{14}$$

The corresponding contact ratio sample is then computed as:

$$\sigma_\mu{}^{[j]} = \frac{\sqrt{f_{c1}^{[j]^2} + f_{c2}^{[j]^2}}}{f_{c3}^{[j]}}, \tag{15}$$

where f_{c1}, f_{c2} are the tangential components of the contact force, f_{c3} is the normal component of the contact force. The probabilistic contact stability metric κ_σ for the given blood flow disturbance is then:

$$\kappa_\sigma = \frac{1}{N_v}\sum_{j=1}^{N_v} U_\sigma(\sigma_\mu{}^{[j]}), \tag{16}$$

where $U_\sigma(y) = 1$ if $0 \le y \le \mu_s$, and 0 otherwise. Analogously, the probabilistic contact safety metric κ_f for the given blood flow disturbance is given by:

$$\kappa_f = \frac{1}{N_v}\sum_{j=1}^{N_v} U_f(f_{c3}^{[j]}), \tag{17}$$

where $U_f(y) = 1$ if $f_{\min} \le y \le f_{\max}$, and 0 otherwise.

The probabilistic contact stability and contact safety metrics can be generalized to the surface motion case in a similar manner. Specifically, consider the heart position samples $\{\Psi(x_0)^{[1]}, \Psi(x_0)^{[2]}, ..., \Psi(x_0)^{[N_x]}\}$ of the point of interest (POI) on tissue surface drawn from the heart motion trajectory. At each position sample $\Psi(x_0)^{[j]}$, a new catheter configuration $X^{[j]}$ is obtained by potential energy minimization (3) and (4), and the corresponding contact Jacobian $J_C^{[j]}$ is updated using (1). The contact force samples are first obtained using (7) as:

$$f_c^{[j]} = {J_C^{[j]T}}^{\dagger} \nabla_X f(u, X^{[j]}), \tag{18}$$

The corresponding contact ratio sample $\sigma_\mu^{[j]}$ under the given position sample can be obtained using (15). The probabilistic contact stability metric κ_σ and contact safety metric κ_f given the surface motion disturbance are then calculated using (16) and (17), respectively.

4 Contact Stability and Safety Analysis — An Example Scenario Under Blood flow and Surface Motion Disturbances

In this analysis scenario, we will investigate how the contact stability and safety metrics vary for three nominal normal contact force levels, namely, at 0.25 N (high), 0.20 N (moderate) and 0.10 N (low), under LIV blood flow disturbances and the left ventricle surface motions with the presence of arrhythmia.

The parameters identified in [14] of our MRI-actuated robotic catheter prototype are used as the parameters of the PRB model in this paper. The PRB model of the robotic catheter has the length of 100 mm, 5 pseudo-rigid links, each with 20 mm length. For evaluation of the contact stability and safety under surface motion disturbances, we have used *in vivo* heart motion data collected in our earlier studies [15]. Specifically, a 128 s long recording of the heartbeat motion (cardiac and respiratory motion) data with the presence of arrhythmia collected from a POI on the left ventricle (LV), sampled at a 404.5 Hz sampling rate, is used (Fig. 2). 51,780 heart motion samples $\{\Psi(x_0)^{[j]}\}$ are then drawn from the 128 s motion data for contact stability and safety analysis.

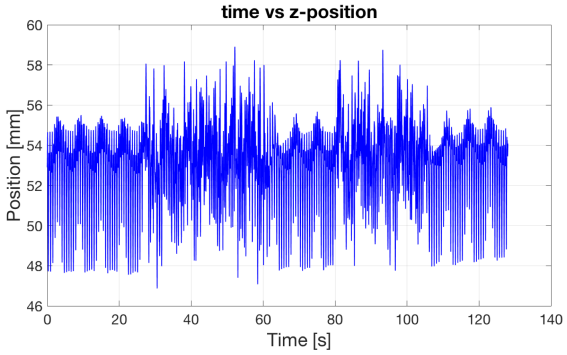

Fig. 2. The z-axis POI position data of the 128 s long heart motion with two arrhythmia occurrences.

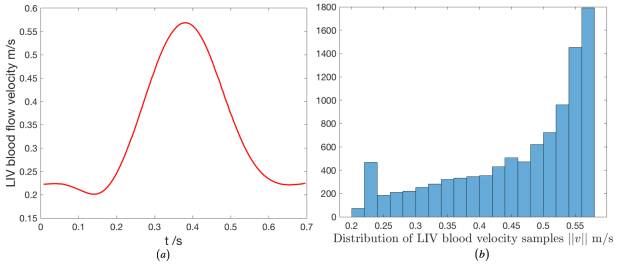

Fig. 3. (a) The left inferior pulmonary vein (LIV) blood flow velocity profile calculated from the data reported in [16] using a distal diameter of 1.8 cm. The minimum and maximum blood flow velocities are 0.21 m/s and 0.57 m/s, respectively. (b) Histogram of the 10,000 blood flow velocity samples drawn from the blood flow velocity profile in (a).

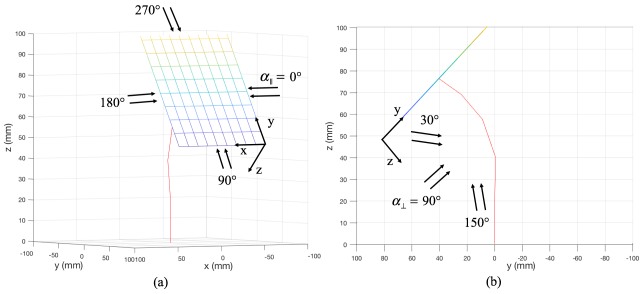

Fig. 4. (a) The illustration of the blood flow directions in the tangential plane. The directional angle $\alpha_{\|}$ is varied in $[0°,\ 360°]$. (b) The illustration of the blood flow directions in the plane perpendicular to the tangential plane at $\alpha_{\|} = 90°$. $\alpha_{\perp}$ is varied in $[30°,\ 150°]$. At $\alpha_{\perp} = 90°$, the blood flow direction is parallel to the tangential plane.

For evaluation of the contact stability and safety under blood flow disturbances, a distribution obtained by sampling of the left inferior pulmonary vein[1] (LIV) blood flow is used

[1]Left inferior pulmonary vein is one of the four pulmonary veins connected to the left atrium and is targeted in the pulmonary vein isolation

as the underlying blood flow velocity distribution. Specifically, 10,000 velocity samples $\{v^{[i]}\}$ are drawn from the left inferior pulmonary vein blood flow velocity profile reported in [16]. The blood density is $\rho = 1.04 \times 10^3 kg/m^3$ [17]. Since the length of each pseudo-link is equal, the drag coefficient C_D for each pseudo-link is given as $C_D = 0.76$ [11].

The blood flow direction varies substantially during the cardiac cycle. Therefore, as part of the analysis to investigate how the blood flow disturbances affect the stability and safety of the catheter-tissue contact, we have also looked at the variation of the contact stability and safety metrics for a range of blood flow directions. Specifically: Let $\alpha_{\parallel}$ denote the direction angle of the blood flow in the tangential plane of the tissue surface at the contact point, and $\alpha_{\perp}$ denote the direction angle in the plane perpendicular to the tangential plane.[2] The blood flow direction w_v in spatial frame is then given as

$$w_v = R_s[\sin(\alpha_{\perp})\cos(\alpha_{\parallel})\ \sin(\alpha_{\perp})\sin(\alpha_{\parallel})\ \cos(\alpha_{\perp})]^T,$$

where $R_s \in SO(3)$ denotes the rotational transformation from the surface frame to the catheter spatial frame. In this study, we consider $\alpha_{\parallel} \in [0^\circ,\ 360^\circ]$ and $\alpha_{\perp} \in [30^\circ,\ 150^\circ]$, as shown in Fig. 4.

In [18], the static friction coefficients of a silicone catheter against aorta and superior vena cava are reported as 0.67 and 0.56, respectively, where blood is used as lubricant for both cases. In this study, we use a relatively conservative value of $\mu_s = 0.2$ as the static friction coefficient between the robotic catheter and the atrial surface [19]. The minimum normal force limit $f_{\min}$ for a safe catheter-tissue contact is given as $f_{\min} = 0.10$ N, and the maximum normal force limit is given as $f_{\max} = 0.25$ N.

First, the contact stability metric κ_σ, and the contact safety metric κ_f are calculated for the nominal normal contact force of 0.10 N (the lower normal force limit), 0.20 N (the moderate normal contact force), and 0.25 N (the upper normal force limit), under the LIV blood flow disturbances for the flow directions being considered. The catheter is actuated to produce the corresponding nominal normal force level in the absence of disturbances using the contact force control algorithm proposed in [20].

The contact analysis results for 0.10 N are presented in Fig. 5 (a) and (b). As shown in Fig. 5 (a), the probabilistic contact stability metric κ_σ is 1 for all considered blood flow directions, indicating a stable contact between the catheter tip and tissue surface under the potential LIV blood flow disturbances. The resulting probabilistic contact safety metric κ_f under the blood flow disturbances are provided in Fig. 5 (b), where the probabilistic contact safety metric κ_f falls below 1 at some directional regions (and actually equals 0 for some directional regions), indicating unsafe catheter-tissue contact forces. As shown in Fig. 5 (c) and (d), given nominal normal force of 0.20 N, both the contact stability and the contact safety metrics are equal to 1 for all considered blood flow directions, indicating stable contact with contact forces within the safe limits. As shown in Fig. 5 (e), with normal force of 0.25 N, the robotic catheter is able to provide a stable catheter-tissue contact over the considered blood flow directions. However, the external torque created by the blood flow disturbances in some directional regions can lead to a normal force higher than the force limit of 0.25 N, pushing the probabilistic contact safety metric κ_f below 1, as shown in Fig. 5 (f).

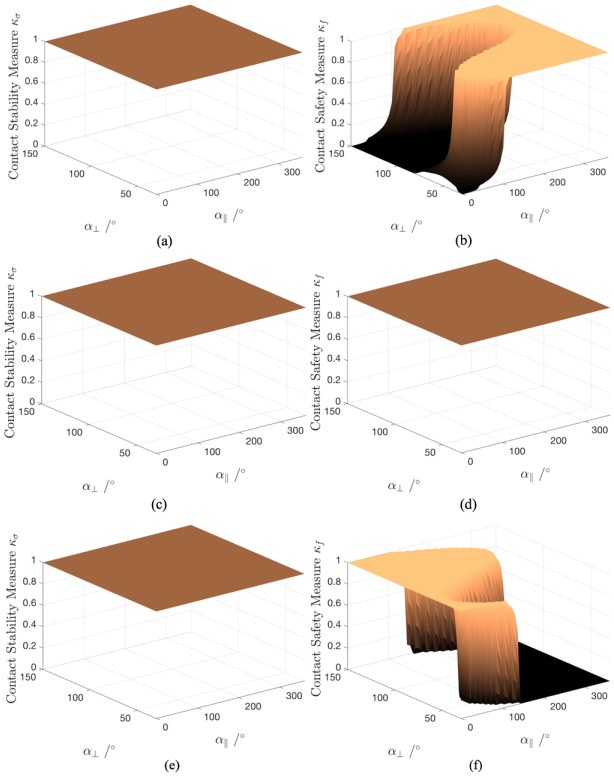

Fig. 5. The probabilistic contact stability metric κ_σ (a) and contact safety metric κ_f (b) given nominal contact normal force magnitude of 0.10 N for blood flow directions $\alpha_{\parallel} \in [0^\circ,\ 360^\circ]$ and $\alpha_{\perp} \in [30^\circ,\ 150^\circ]$. The probabilistic contact stability metric κ_σ (c) and contact safety metric κ_f (d) given nominal contact normal force magnitude of 0.20 N for blood flow directions $\alpha_{\parallel} \in [0^\circ,\ 360^\circ]$ and $\alpha_{\perp} \in [30^\circ,\ 150^\circ]$. The probabilistic contact stability metric κ_σ (e) and contact safety metric κ_f (f) given nominal contact normal force magnitude of 0.25 N for blood flow directions $\alpha_{\parallel} \in [0^\circ,\ 360^\circ]$ and $\alpha_{\perp} \in [30^\circ,\ 150^\circ]$.

The contact stability and contact safety of the robotic catheter under the left ventricle surface motions with the presence of arrhythmia are then investigated. The resulting contact ratios and normal contact forces over the 51,780 heart motion samples are calculated, as presented in Fig. 6.

As shown in Fig. 6, the stability and safety of the catheter-tissue contact achieved by the three nominal normal forces cannot be guaranteed under the surface motion disturbances. The robotic catheter is not able to provide stable catheter-tissue contact under the provided nominal normal

technique of the atrial fibrillation ablation procedure.

[2] $\alpha_{\parallel}$ and $\alpha_{\perp}$ can be thought as the azimuth and elevation angles for the blood flow direction relative to the tissue tangent surface at the catheter tip.

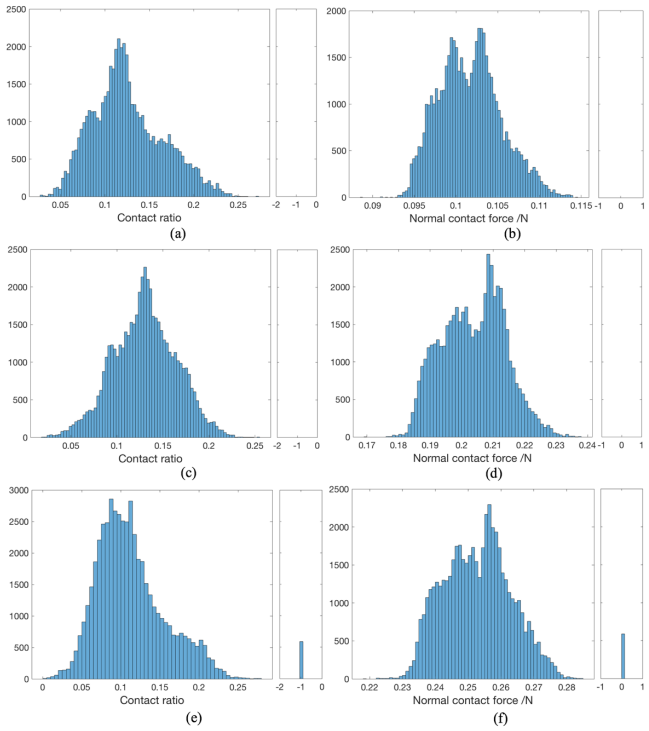

Fig. 6. Contact ratio distribution for the 51,780 heart motion samples for given nominal normal force of 0.10 N (a), 0.20 N (c), and 0.25 (e). Normal contact force distribution for the 51,780 motion samples for given nominal normal force of 0.10 N (b), 0.20 N (d), and 0.25 (f). The side plots denote the number of motion samples that lost contact with the catheter tip.

forces, as the contact ratios exceeded the friction coefficient. The catheter tip-tissue contact is unsafe under the nominal normal force of 0.10 N and 0.25 N. Using the nominal normal force of 0.25 N, the robotic catheter lost contact with the tissue surface for some motion samples, as shown in Fig. 6 (e) and (f), where the normal forces become 0 and the corresponding contact ratios are marked as -1.

5 Discussion and Conclusion

Understanding and analyzing the effects of cardiac surface motions and blood flow on stability and safety of catheter-tissue contact is crucial for development of robotic intracardiac catheter systems. In this paper, a probabilistic formulation of the contact stability and contact safety is proposed. A probabilistic blood flow disturbance model is introduced, where a quasi-static model are employed for approximating the blood flow drag forces applied on the catheter body. The probabilistic contact stability and contact safety metrics, employing a sample based representation of the surface motion trajectory and blood flow velocity distribution, are defined. The proposed models and metrics are then employed in an example scenario to analyze the catheter-tissue contact stability and safety for a MRI-actuated robotic catheter in a specific catheter-tissue contact configuration. It is important to note that the specific contact safety and contact stability analysis presented in Section 4 is intended as an illustration of the methods proposed, rather than for making generalizable conclusions of a specific robotic catheter or controller. Specific analysis would typically be performed with patient specific data for anatomy, blood flow, and catheter configuration, etc..

Although the employed MRI-actuated robotic catheter system was considered as the underlying example robotic catheter platform throughout the paper, the proposed models and methods are broadly applicable to other types of intracardiac robotic catheters, as long as appropriate Jacobians are available. Additionally, the proposed probabilistic formulation of the contact stability and safety can be applied to a combined disturbance model integrating the surface motion and blood flow disturbances, for example, the left atrium surface motion and LIV blood flow disturbances, if correlated data is available.

References

[1] Liu, T., Poirot, N. L., Franson, D., Seiberlich, N., Griswold, M. A., and Cavusoglu, M. C., 2016. "Modeling and validation of the three-dimensional deflection of an mri-compatible magnetically actuated steerable catheter.". *IEEE Trans. Biomed. Engineering,* **63**(10), pp. 2142–2154.

[2] Liu, T., and Çavuşoğlu, M. C., 2014. "Three dimensional modeling of an mri actuated steerable catheter system". In Robotics and Automation (ICRA), 2014 IEEE International Conference on, IEEE, pp. 4393–4398.

[3] Reddy, V. Y., Shah, D., Kautzner, J., Schmidt, B., Saoudi, N., Herrera, C., Jaïs, P., Hindricks, G., Peichl, P., Yulzari, A., et al., 2012. "The relationship between contact force and clinical outcome during radiofrequency catheter ablation of atrial fibrillation in the toccata study". *Heart rhythm,* **9**(11), pp. 1789–1795.

[4] Thiagalingam, A., D'AVILA, A., Foley, L., Guerrero, J. L., Lambert, H., Leo, G., Ruskin, J. N., and Reddy, V. Y., 2010. "Importance of catheter contact force during irrigated radiofrequency ablation: evaluation in a porcine ex vivo model using a force-sensing catheter". *Journal of cardiovascular electrophysiology,* **21**(7), pp. 806–811.

[5] Sohns, C., Karim, R., Harrison, J., Arujuna, A., Linton, N., Sennett, R., Lambert, H., Leo, G., Williams, S., Razavi, R., et al., 2014. "Quantitative magnetic resonance imaging analysis of the relationship between contact force and left atrial scar formation after catheter ablation of atrial fibrillation". *Journal of cardiovascular electrophysiology,* **25**(2), pp. 138–145.

[6] Williams, S. E., Harrison, J., Chubb, H., Bloch, L. Ø., Andersen, N. P., Dam, H., Karim, R., Whitaker, J., Gill, J., Cooklin, M., et al., 2015. "The effect of contact force in atrial radiofrequency ablation: electroanatomical, cardiovascular magnetic resonance, and histological assessment in a chronic porcine model". *JACC: Clinical Electrophysiology,* **1**(5), pp. 421–431.

[7] Hao, R., Lombard Poirot, N., and Cavusoglu, M. C., 2020. "Analysis of contact stability and contact safety of a robotic intravascular cardiac catheter under blood flow disturbances". In Proceedings of the IEEE/RSJ International Conference on Intelligent Robots and Systems (IROS 2020).

[8] Murray, R. M., 2017. *A mathematical introduction to robotic manipulation*. CRC press.

[9] Greigarn, T., Poirot, N. L., Xu, X., and Cavusoglu, M. C., 2018. "Jacobian-based task-space motion planning for mri-actuated continuum robots". *IEEE Robotics and Automation Letters*.

[10] Ku, D. N., 1997. "Blood flow in arteries". *Annual review of fluid mechanics,* **29**(1), pp. 399–434.

[11] Nakayama, Y., 2018. *Introduction to fluid mechanics*. Butterworth-Heinemann.

[12] Huston, R. L., and Kamman, J. W., 1981. "A representation of fluid forces in finite segment cable models". *Computers & Structures,* **14**(3-4), pp. 281–287.

[13] Thrun, S., Burgard, W., and Fox, D., 2005. *Probabilistic robotics*. MIT press.

[14] Greigarn, T., 2018. "Kinematics, planning, and perception for magnetically-actuated MRI-guided continuum robots". PhD thesis, Case Western Reserve University.

[15] Tuna, E. E., Franke, T. J., Bebek, O., Shiose, A., Fukamachi, K., and Cavusoglu, M. C., 2012. "Heart motion prediction based on adaptive estimation algorithms for robotic-assisted beating heart surgery". *IEEE Transactions on Robotics,* **29**(1), pp. 261–276.

[16] Qureshi, M. U., Vaughan, G. D., Sainsbury, C., Johnson, M., Peskin, C. S., Olufsen, M. S., and Hill, N., 2014. "Numerical simulation of blood flow and pressure drop in the pulmonary arterial and venous circulation". *Biomechanics and modeling in mechanobiology,* **13**(5), pp. 1137–1154.

[17] Cameron, J., Skofronick, J., and Grant, R., 1999. *Physics of the Body*. Medical Physics Series. Medical Physics Pub.

[18] Prokopovich, P., Perni, S., Piccirillo, C., Pratten, J., Parkin, I. P., and Wilson, M., 2010. "Frictional properties of light-activated antimicrobial polymers in blood vessels". *Journal of Materials Science: Materials in Medicine,* **21**(2), pp. 815–821.

[19] Liu, T., Poirot, N., Greigarn, T., and Cavusoglu, M., 2017. "Design of an MRI-guided magnetically-actuated steerable catheter". *ASME Journal of Medical Devices, Special Issue on Cardiovascular Device Development and Safety Assessment using Computational and/or Experimental Approaches,* **11**.

[20] Hao, R., Greigarn, T., and Çavuşoğlu, M. C., 2020. "Contact stability analysis of magnetically-actuated robotic catheter under surface motion". In *IEEE International Conference on Robotics and Automation*.